JCTC Journal of Chemical Theory and Computation

Simulating the Transition between Gel and Liquid-Crystal Phases of Lipid Bilayers: Dependence of the Transition Temperature on the Hydration Level

Bruno A. C. Horta,*,† Alex H. de Vries,‡ and Philippe H. Hünenberger*,†

Laboratory of Physical Chemistry, ETH Zürich, CH-8093 Zürich, Switzerland, and University of Groningen, Nijenborgh 4, 9747 AG Groningen, The Netherlands

Received April 14, 2010

Abstract: Explicit-solvent molecular dynamics (MD) simulations of the monoglyceride glycerol-1-monopalmitin (GMP; bilayer patch of 2 × 6 × 6 lipids) at different hydration levels (full, half, or quarter hydration) and at different temperatures (318 to 338 K) are reported. The 40 ns simulations (some extended to 200 ns) are initiated from structures appropriate for the gel (GL) or liquid-crystal (LC) phases, with the goal of investigating whether atomistic MD simulations on this time scale can be used to monitor GL ↔ LC transitions in lipid bilayers, and to evaluate the corresponding transition temperatures T_m (as well as the influence of hydration on T_m) in a reliable fashion. The main conclusions are as follows: (*i*) The GL → LC transition of GMP can be observed on the 40 ns time scale. (*ii*) The LC → GL transition is comparatively slower, requiring simulations on the 200 ns time scale. (*iii*) A set of simulations initiated from a structure appropriate for the GL phase and carried out at slightly different temperatures permits the determination of a reliable value for T_m. (*iv*) The calculated T_m values reproduce the experimentally observed increase in this transition temperature upon decreasing the bilayer hydration. (*v*) The T_m values calculated at the three hydration levels considered are in essentially quantitative agreement with the experimental phase diagram of GMP. To our knowledge, this study represents the first accurate determination of the T_m of a lipid *via* atomistic simulations of the (reversible) GL ↔ LC phase transition, as well as the first direct simulation evidence for the increase in the transition temperature upon dehydration. The possible direct determination of T_m and the characterization of environmental effects on this quantity by simulation opens up promising perspectives in the contexts of force field refinement and the investigation of dehydration-induced damages in living cells (and bioprotection by cosolutes).

I. Introduction

Lipid bilayers are known to exist in several different lyotropic phases,[1,2] the relative stabilities of which depend on the temperature and pressure conditions, on the type of lipid molecules, on the identity and concentration of the solvent, and on the nature and concentration of possible cosolutes.[1,2] The most important and best studied of these phases are the crystal phases, the gel phases, and the liquid-crystal phase.[1] Different crystal and gel phases may be further distinguished, depending on the specific (regular) arrangement of the lipid molecules.

Crystal (CR) phases can be viewed as resulting from the periodic stacking of nearly dehydrated bilayers (except for the possible presence of a limited number of cocrystallization water molecules), in which the aliphatic lipid tails are arranged regularly in *all-trans* conformations.[1,2] These phases have a limited biological relevance, but polymorphism and crystallization phenomena are particularly important for the

* Corresponding authors. Phone: +41 44 632 5503. Fax: + 41 44 632 1039. E-mail: bruno.horta@gmail.com (B.A.C.H.), phil@igc.phys.chem.ethz.ch (P.H.H.).

† Laboratory of Physical Chemistry.

‡ University of Groningen.

10.1021/ct100200w
Published on Web 07/20/2010

food and pharmaceutical industries.[2] The crystal structures of numerous types of lipids have been solved by solid-state X-ray diffraction and have revealed interesting symmetry, enantiomerism, and polymorphism properties.[1−10]

Gel (GL) phases (in multilamellar systems) can be viewed as resulting from the regular (but not strictly periodic) stacking of significantly hydrated bilayers, in which the aliphatic lipid tails are arranged in nearly *all-trans* conformations and in orientations that are generally tilted with respect to the bilayer normal.[1] Due to the separation of successive bilayers by solvation shells, there is no or very little correlation between the arrangement of the lipids (e.g., tilting direction or undulations) in successive bilayers. Although the GL phase represents a highly ordered bilayer state, it is undoubtedly much more "dynamical" than the CR phase. This phase is not predominant in biological systems, although some evidence points toward the existence of small gel-like domains in cell membranes.[1,2]

The liquid-crystal (LC) phase (sometimes called fluid phase) also consists of significantly hydrated bilayers, but in which the aliphatic tails are conformationally disordered. Other structural and dynamic properties differentiating the LC from the GL phase are a broader distribution of the headgroup atoms along the bilayer normal, a larger area per lipid, a smaller bilayer thickness, and faster translational and rotational diffusion of the lipid molecules. Due to the highly disordered and "dynamical" (fluid-like) structure, many processes of biological importance can take place within a bilayer in the LC phase (e.g., insertion of macromolecules, transport, fusion, signaling). However, for the same reason, it is much more difficult to accurately measure structural properties of the LC phase compared to the more ordered CR and GL phases.[11]

The transition of a lipid bilayer from the LC phase to a more ordered (GL or CR) phase can be promoted by a temperature decrease (at constant water content). The temperature T_m at which this transition occurs (for a given water content) is referred to as the main transition temperature. Alternatively, the same transition can typically be promoted by dehydration (at constant temperature). In practice, however, the phase diagrams of lipid−water systems are generally complicated by the existence of other phases and by the slow kinetics associated with specific phase transitions, rendering sometimes difficult the clear-cut distinction between stable and metastable phases.

From the biological point of view, the LC ↔ GL phase transition is particularly important. Although the biologically relevant phase of cell membranes is considered to be the LC phase, the cholesterol-rich regions of this membrane may form small organized domains, in which the ordering approaches that of a GL phase.[12,13] This process is related to the formation of membrane rafts, which has been suggested to play a major role in cell signaling,[14−16] protein transport and association,[15] and other functions such as toxin binding.[17] Under stressful environmental conditions (e.g., low temperature or dehydration),[18,19] biological membranes can suffer undesirable phase transitions (e.g., LC → GL transition of a large portion of the membrane), leading to the loss of their biological function and, in more drastic situations, to the disruption of the membrane (upon reheating or rehydration). Many organisms have developed molecular strategies to prevent this transition, typically by adjusting the concentration of specific cosolutes (e.g., sugars) in the cell.[19−26] The lyotropic phase transitions are also important for many industrial processes such as food production and conservation and cosmetics and pharmaceutical formulations, as well as nanomaterials and synthetic applications.[1,27,28] Due to the great practical relevance of the problem, many experimental techniques have been developed for the accurate identification of lipid phases and the characterization of the corresponding transitions.[29−31]

Computer simulations have also greatly contributed to the characterization and understanding of the structure, dynamics, and thermodynamics of lipid bilayers. Among these methods, molecular dynamics (MD) simulation has proved to be particularly useful, because it provides information at a spatial (atomic level) and temporal (femtosecond) resolution inaccessible to experimentation, concerning system sizes (∼10 nm scale) and time scales (∼10−100 ns) still relevant for the evaluation of thermodynamic properties (statistical mechanics) and comparison with experimental data. Due to its biological relevance and to historical controversies concerning derived experimental data (e.g., value of the area per lipid,[11] possible presence of a surface tension[32,33]), many simulation studies have focused on the characterization of the LC phase.[34−39] However, some studies have also considered GL phases,[35,40−43] as well as other less common (but not less interesting) phases (e.g., ripple phase,[44] cubic phase[45,46]). On the other hand, although statistical models[47] and coarse-grained simulations[13] have been applied to characterize the GL ↔ LC transition, atomistic MD simulations that systematically investigate this process are scarce. The main reason is the relatively long time scale associated with this phase transition, which requires undertaking very long simulations. However, nowadays, time scales of 10−100 ns have become accessible for atomistic simulations considering systems with several thousand atoms. It is thus possible to simulate phase transitions of lipid−water systems in favorable cases, i.e., for systems where the equilibration of the individual phases occurs within time scales on this order. In the case of phospholipids, the time scale required for obtaining a fully equilibrated structure for the LC phase, which is a lower bound for the LC ↔ GL transition time scale, is already on the order of several nanoseconds.[48] For this reason, it may be more appropriate to study less complex bilayer systems such as surfactant or monoglyceride lipid systems. Since these have only one aliphatic tail per headgroup, their conformational and orientational relaxation is significantly faster, and convergence can be reached in comparatively shorter simulations.

In a recent study, Debnath et al.[49] reported MD simulations of a charged surfactant−cosurfactant system investigating the influence of the bilayer composition on the GL → LC transition. Different hydration levels were considered (50 and 80% w/w water concentrations), but no significant differences in the transition behavior were observed (in agreement with experimental results, given the high water content considered).

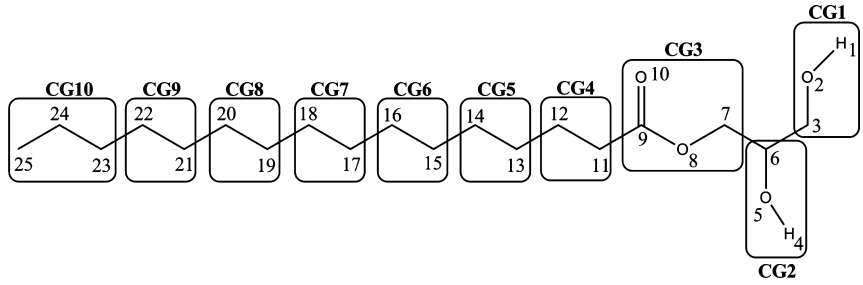

Figure 1. Chemical structure of the monoglyceride considered in the present study, glycerol-1-monopalmitate (GMP). The numbering refers to the GROMOS molecular topology. The charge group (CG) definitions are also indicated (all CGs are overall neutral). The methylene (11−24) and methyl (25) groups of the acyl chain are represented by united atoms with zero partial charge. The partial charges used for the headgroup atoms are reported in Table 1.

In the present study, the effect of the hydration level on the GL ↔ LC transition is investigated systematically, in the context of a saturated monoglyceride system. A monoglyceride is the molecule resulting from the esterification of a hydroxyl group of glycerol with a fatty acid. Monoglycerides present a number of key advantages, compared to, e.g., dipalmitoylphosphatidylcholine (DPPC), for a computational investigation of the GL ↔ LC phase transition: (*i*) the presence of only one aliphatic tail per headgroup, leading to a faster conformational and rotational relaxation; (*ii*) the limited role of long-range electrostatic interactions (uncharged, nonzwitterionic, and moderately polar headgroups), also leading to a faster relaxation and largely avoiding artifacts related to the approximate treatment of electrostatic interactions and the limited system size in simulations;[50−59] (*iii*) the absence of a ripple phase[44] as an intermediate state between the GL and the LC phases; and (*iv*) the availability of experimental structural and thermodynamic data.[60−69] More specifically, glycerol-1-monopalmitate (GMP; Figure 1) was chosen here as a model lipid, due to the availability of an experimental phase diagram.[69]

The phase diagram of the racemic GMP−water system[69] (as a function of hydration level and temperature, at pressure $P = 1$ atm) is reproduced in Figure 2. If a sample of GMP in the CR phase is heated in the presence of water at a concentration of about 30% w/w, the melting of the crystals and the formation of a LC phase is observed at about 55 °C. If the system is then cooled down relatively fast, a GL phase is formed at a temperature of about 50 °C. The GL phase is metastable and converts into a stable coagel (biphasic system consisting of CR and water phases), although this transformation only occurs over a period of a few hours (or even days). Note that this process is further complicated by the presence of polymorphism in the CR phase.

In this article, a total of 24 atomistic MD simulations (40−200 ns) of a racemic GMP bilayer patch performed at different temperatures and hydration levels, and starting from different initial conditions, are reported and compared. The main goal of this work is to investigate whether such simulations can account for (*i*) the GL → LC transition, the associated temperature T_m, and the increase of T_m upon decreasing the hydration level below about 20% w/w (Figure 2); (*ii*) the corresponding LC → GL transition, *a priori* more difficult to capture (disorder → order transition); and (*iii*) the main structural and dynamic properties of the GL and LC phases.

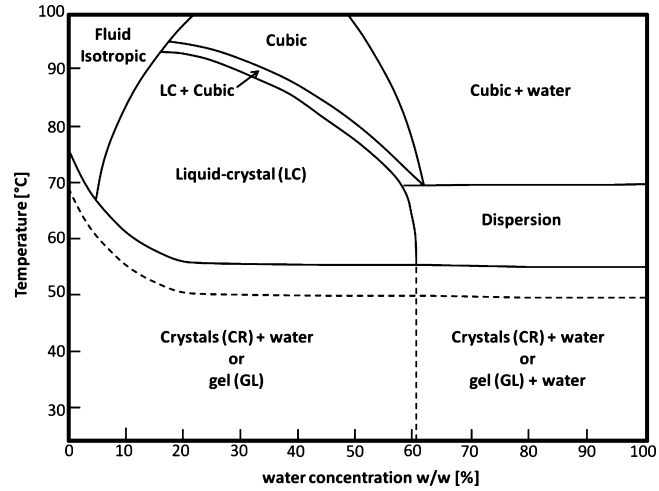

Figure 2. Phase diagram of the binary system glycerol-1-monopalmitate (GMP)−water. The horizontal axis represents the water concentration (in percent, weight-to-weight) and the vertical axis the temperature. Solid lines indicate equilibrium phase transitions, while the dashed line indicates the transitions involving the metastable GL phase (GL → LC and LC → GL). The phase diagram was adapted with permission from ref 69, copyright 1968, Elsevier.

II. Computational Details

II.1. Molecular Dynamics Simulations. All MD simulations were performed using the GROMOS96 program[70,71] together with a slightly modified version of the GROMOS 53A5 force field[72] for the lipids and the simple point charges (SPC) water model.[73] The only adjustment made to the original 53A5 force field concerns the partial charges of the headgroup atoms, which are reported in Table 1. These charges originated from an intermediate step in the parametrization of the new $53A6_{OXY}$ force field,[74] calibrated to reproduce experimental thermodynamic properties of oxygen compounds (alcohols, ethers, aldehydes, ketones, carboxylic acids, and esters). These charges were further slightly modified in an independent set of simulations (data not shown) to bring the equilibrium area per lipid as close as possible to the experimental values for both the GL and LC phases of GMP. The simulations were carried out under periodic boundary conditions based on rectangular boxes containing a hydrated GMP lipid bilayer patch of $2 \times 6 \times 6$ lipid molecules (in the *xy* plane, i.e., normal to the *z* axis). Newtons equations of motion were integrated using the

Table 1. Comparison between the Original 53A5 Charges for the Headgroup of GMP and the Modified Charges Used in the Present Study

charge group[a]	chemical function	atom label[a]	atom type[b]	IAC[b]	partical charges [*e*] original 53a5	partical charges [*e*] this work
1	alcohol	1	H	21	0.403	0.410
		2	OA	3	−0.611	−0.642
		3	CH2	15	0.208	0.232
2	alcohol	4	H	21	0.403	0.410
		5	OA	3	−0.611	−0.642
		6	CH1	14	0.208	0.232
3	ester	7	CH2	15	0.16	0.24
		8	OE	4	−0.36	−0.36
		9	C	12	0.58	0.66
		10	O	1	−0.38	−0.54

[a] Charge groups and atom labels are shown graphically in Figure 1. [b] Atom types and integer atom codes (IAC) refer to the 53A5 force field article.[72]

leapfrog scheme[75] with a time step of 2 fs. All bond lengths were constrained using the SHAKE procedure[76] with a relative geometric tolerance of 10^{-4}. The center of mass motion was removed every 100 ps. The simulations were performed in the *NPT* ensemble (constant number of particles N, pressure P, and temperature T) with a reference pressure $P = 1$ bar, and reference temperatures T ranging from 318 to 338 K. The temperature was maintained by weakly coupling the solute and solvent degrees of freedom separately to a temperature bath[77] at temperature T, with a relaxation time of 0.1 ps. The pressure was maintained by weakly coupling the particle coordinates and box dimensions in the xy plane and along the z axis separately[78] to a pressure bath at pressure P, with a relaxation time of 0.5 ps and an isothermal compressibility of 4.575×10^{-4} (kJ mol^{-1} nm^{-3})$^{-1}$ as appropriate for water.[70] The nonbonded interactions were computed using a twin-range scheme,[70,79] with short- and long-range cutoff distances set to 0.8 and 1.4 nm, respectively, and a frequency of five time steps for the update of the short-range pairlist and intermediate-range interactions. A reaction-field correction[80,81] was applied to account for the mean effect of electrostatic interactions beyond the long-range cutoff distance, using a relative dielectric permittivity of 61 as appropriate for the SPC water model.[82] Configurations were saved every 5 ps for analysis.

II.2. Simulated Systems. All simulations were carried out starting from two different initial (equilibrated) bilayer structures at full hydration (see below), one corresponding to a GL phase (I_{GL}) and the other one to a LC phase (I_{LC}). These structures were generated from exisiting snapshots of double-tailed DPPC phospholipids by reordering the atoms and deleting superfluous headgroup atoms, so as to map the two tail-to-tail DPPC molecules onto two tail-to-tail GMP molecules. The molecules were then placed in a box of lateral dimensions 0.6×0.6 nm and periodically replicated on a 6×6 lateral lattice to form a bilayer structure with 36 lipids per monolayer. Water molecules were added to the system by random insertion. The reference improper-dihedral controlling the chirality of the substituted glycerol moiety was set to opposite values for half of the lipid molecules in each leaflet, so as to generate a racemic bilayer (18 *R* and 18 *S* lipid molecules per leaflet). Water molecules initially inserted in the bilayer interior region were removed. Energy minimization and gentle equilibration provided the starting structure representative of the LC systems. The starting structure for the GL systems was obtained from a run of a LC system at a low temperature (308 K) during which the gel-like structure formed spontaneously. The run was continued at 318 K for 50 ns to further equilibrate this structure. Three different hydration levels were considered, which will be referred to as "full", "half", and "quarter" hydration. In the three cases, the computational box contained 72 lipid molecules along with 480 (full; 36.4% w/w), 240 (half; 18.2% w/w), or 120 (quarter; 9.1% w/w) water molecules. The simulations at full hydration were started directly from systems I_{GL} or I_{LC}. The initial coordinates of the systems at half hydration (I^{H}_{GL} and I^{H}_{LC}) were generated from configurations I_{GL} and I_{LC} *via* deletion of an appropriate number of water molecules (most remote from the bilayer midplane) and re-equilibration by 4 ns MD with positionally constrained lipid atoms (at constant normal pressure $P_z = 1$ bar and temperature $T = 338$ K). The same procedure was applied to generate the initial coordinates for the systems at quarter hydration (I^{Q}_{GL} and I^{Q}_{LC}) from those at half hydration (I^{H}_{GL} and I^{H}_{LC}).

Starting from the six initial configurations (I_{GL}, I_{LC}, I^{H}_{GL}, I^{H}_{LC}, I^{Q}_{GL}, and I^{Q}_{LC}), production simulations were preceded by energy minimization and a second MD equilibration (0.5 ns) to heat up the systems to the appropriate temperatures (318 K for the gel phase and 338 K for the LC phase) in the presence of progressively decreasing position restraints on the lipid atoms. From this point on, eight 40 ns production simulations were performed, at each of the three hydration levels: 3×6 simulations were started from the GL phase configurations and carried out at temperatures $T = 318$, 322, 326, 330, 334, or 338 K; 3×2 simulations were started from the LC phase configurations and carried out at temperatures $T = 318$ or 338 K. Each of the 24 production simulations will be referred to by a unique label characterizing the hydration level, initial bilayer structure, and reference simulation temperature. The labels, simulated systems, and simulation conditions are summarized in Table 2. Note that the average temperature in the simulated systems ($\langle T \rangle$ in Table 2) may slightly differ from the corresponding reference (thermostat) temperatures T. However, since the differences are of at most 1.8 K, they can be neglected, and the discussion will be performed in terms of T for simplicity.

II.3. Trajectory Analysis. The simulations were analyzed in terms of area per lipid a_{xy}, order parameters $S_{CH}(C_n)$ of the 14 methylene groups (C_n, with $n = 2-15$; atom numbers in Figure 1 minus nine), average number of *gauche* conformations per chain (n_G), average numbers (N) of intermolecular hydrogen bonds (H-bonds) between the different species, lipid lateral diffusion coefficients (D_{xy}), and lipid rotational (R) or wobbling (W) relaxation times τ and residual correlations c (τ_1^R, c_1^R, τ_2^R, c_2^R, τ_1^W, c_1^W, τ_2^W, c_2^W; distinguishing fast and slow decays by the indexes 1 and 2).

The area per lipid a_{xy} was calculated as the surface of the computational box in the xy plane divided by 36 and monitored as a function of time (indicator of a phase

Table 2. Simulated Systems and Simulation Conditions[a]

	hydration level					
label	hydration	c_{H_2O} [% w/w]	n_{H_2O}	starting configuration	T [K]	$\langle T \rangle$ [K]
$F_{GL}318$	full	36.4	480	GL	318	317.2
$F_{GL}322$	full	36.4	480	GL	322	321.1
$F_{GL}326$	full	36.4	480	GL	326	325.3
$F_{GL}330$	full	36.4	480	GL	330	329.3
$F_{GL}334$	full	36.4	480	GL	334	333.3
$F_{GL}338$	full	36.4	480	GL	338	337.3
$F_{LC}318$	full	36.4	480	LC	318	317.1
$F_{LC}338$	full	36.4	480	LC	338	337.3
$H_{GL}318$	half	18.2	240	GL	318	316.4
$H_{GL}322$	half	18.2	240	GL	322	320.4
$H_{GL}326$	half	18.2	240	GL	326	324.5
$H_{GL}330$	half	18.2	240	GL	330	328.6
$H_{GL}334$	half	18.2	240	GL	334	332.7
$H_{GL}338$	half	18.2	240	GL	338	336.6
$H_{LC}318$	half	18.2	240	LC	318	316.7
$H_{LC}338$	half	18.2	240	LC	338	336.6
$Q_{GL}318$	quarter	9.1	120	GL	318	316.3
$Q_{GL}322$	quarter	9.1	120	GL	322	320.3
$Q_{GL}326$	quarter	9.1	120	GL	326	324.3
$Q_{GL}330$	quarter	9.1	120	GL	330	328.2
$Q_{GL}334$	quarter	9.1	120	GL	334	332.2
$Q_{GL}338$	quarter	9.1	120	GL	338	336.3
$Q_{LC}318$	quarter	9.1	120	LC	318	316.4
$Q_{LC}338$	quarter	9.1	120	LC	338	336.3

[a] For each of the 24 simulations, the simulation label, hydration extent (relative to full hydration), water concentration (c_{H_2O}), number of water molecules in the computational box (n_{H_2O}), starting configuration (GL, gel; LC, liquid-crystal), reference (thermostat) temperature (T), and average (overall simulation) temperature ($\langle T \rangle$) are reported. In all cases, the computational box contains $2 \times 6 \times 6$ lipid molecules, and the simulation is carried out for 40 ns at a reference pressure $P = 1$ bar.

transition) or averaged over the last 10 ns of the simulations (structural characteristic of the final states).

The order parameters S_{CH} of the hydrocarbon chains were calculated for the 14 methylene groups of the acyl chains of all GMP molecules, by computing the correlation functions describing the reorientation of the carbon−hydrogen vectors as described elsewhere[83] (see also ref 35). The values of S_{CH} were averaged over the 72 GMP molecules and monitored as a function of time (average S_{chn} over the 14 methylene groups as calculated from 1 ns time windows; indicator for a phase transition) or averaged over the last 10 ns of the simulations ($S_{CH}(C_n)$ or chain averaged value S_{chn}^{end}; structural characteristic of the final state).

The number n_G of *gauche* conformations per chain was calculated on the basis of the time-series of the 12 corresponding dihedral angles and averaged over the 72 lipid molecules and over time (last 10 ns). Because the distributions of the three staggered conformers in the hydrocarbon chains of lipids within bilayers are typically broad,[48,84] all dihedral angles in the ranges 0−120° (*gauche*+) and 240−360° (*gauche*−) were considered to be *gauche*.

The presence of a H bond was defined by a maximal hydrogen−oxygen distance of 0.25 nm and a minimal oxygen−hydrogen−oxygen angle of 135°. The occurring intermolecular H bonds were classified according to the different pairs of species present in the simulations (intralayer lipid−lipid N_{LL}^{intra}, interlayer lipid−lipid N_{LL}^{inter}, lipid−water N_{LW}, and water−water N_{WW}). Average numbers of H bonds were calculated considering the last 10 ns of the simulations.

The lipid lateral diffusion coefficients D_{xy} were calculated from the (average) mean-square displacement curves

$$\Delta(t) = \frac{1}{n_L}\sum_{i=1}^{n_L} \langle [\mathbf{r}_i(t+\tau) - \mathbf{r}_i(t)]^2 \rangle_{\tau \le t_{av}-t}$$

where n_L is the number of lipid molecules (72), $\mathbf{r}_i$ stands for the coordinate vector of the center of geometry of lipid molecule i in the xy plane (two-dimensional vector; including displacements accross periodic boundaries), and the angular brackets indicate averaging over trajectory configurations considering all possible time origins τ (with the condition $\tau \le t_{av} - t$, where t_{av} is the duration of the averaging block). According to the Einstein model,[85] $\Delta(t)$ should be approximately linear, with a slope equal to $4D_{xy}$ (two-dimensional motion). In practice, deviations from linearity are observed at short times (cage effect) and at long times (statistical error). In the present study, the diffusion coefficients (along with error estimates) were evaluated as proposed by Essmann and Berkowitz.[86] The last 12 ns of each trajectory was divided into four 3 ns blocks, for which the diffusion coefficients were calculated by least-squares fit (LSF) to $\Delta(t)$ considering only the interval between 0.3 and 0.5 ns (where the function is close to linear). The D_{xy} value was obtained by averaging the four estimates, and the associated error was estimated by the corresponding standard deviation.

The rotational (R) and wobbling (W) motions of the lipid molecules were analyzed on the basis of the (average) autocorrelation function

$$C(t) = \frac{1}{n_L}\sum_{i=1}^{n_L} \langle \mathbf{v}_i(t+\tau)\cdot\mathbf{v}_i(\tau) \rangle_{\tau \le t_{av}-t}$$

where $\mathbf{v}_i$ is a unit vector characterizing the specific orientational property of lipid molecule i. The rotational motion of the lipids around their main axis was analyzed by considering the unit vector $\mathbf{v}_i$ along the C_9-O_{10} bond (Figure 1; carbonyl group). The wobbling motion was analyzed by considering the unit vector $\mathbf{v}_i$ along the C_9-C_{19} bond (Figure 1; along the aliphatic tail). The relaxation times (τ) and residual correlations (c) of these two modes were obtained by a LSF analysis of the logarithm of the corresponding $C(t)$ function. Both a fast and a slow decay were observed. The fast decay (τ_1^R, c_1^R, τ_1^W, c_1^W) was characterized by $C(t)$ in the interval t = 0−250 ps. The slow decay (τ_2^R, c_2^R, τ_2^W, c_2^W) was characterized by $C(t)$ in the interval t = 250 and 1500 ps. The analysis was performed by considering the last 20 ns of the simulations.

III. Results and Discussion

III.1. Characterization of the GL and LC Phases. Since the present study reports (to our knowledge) the first investigation of GMP bilayers by simulation, it is useful to first briefly discuss the main structural and dynamic properties of the GL and LC phases of this monoglyceride. To this purpose, the simulations $F_{GL}318$ and $F_{LC}338$ corresponding

Table 3. Structural Properties Averaged over the Last 10 ns of the Simulations[a]

label	phase (after 20 ns)	a_{xy} [nm^2]	S_{chn}^{end}	number of *gauche*/chain	H bonds			
					N_{LL}^{intra}	N_{LL}^{inter}	N_{LW}	N_{WW}
$F_{GL}318$	GL	0.248	0.276	1.7	143	0	156	1431
$F_{GL}322$	GL	0.249	0.277	1.8	142	0	155	1421
$F_{GL}326$	LC	0.286	0.210	2.9	120	0	183	1372
$F_{GL}330$	LC	0.291	0.204	3.0	120	0	182	1361
$F_{GL}334$	LC	0.294	0.199	3.0	117	0	185	1347
$F_{GL}338$	LC	0.293	0.195	3.1	117	0	182	1340
$F_{LC}318$	GL	0.251	0.261	1.5	141	0	159	1426
$F_{LC}338$	LC	0.296	0.194	3.1	118	0	181	1340
$H_{GL}318$	GL	0.240	0.278	1.4	148	0	147	640
$H_{GL}322$	GL	0.241	0.278	1.5	149	0	145	637
$H_{GL}326$	GL	0.243	0.276	1.6	144	0	150	626
$H_{GL}330$	GL	0.247	0.267	1.9	141	0	153	617
$H_{GL}334$	LC	0.297	0.191	3.0	118	3	181	571
$H_{GL}338$	LC	0.303	0.182	3.1	115	4	182	564
$H_{LC}318$	Int	0.275	0.229	2.7	126	2	178	599
$H_{LC}338$	LC	0.309	0.173	3.1	113	4	184	560
$Q_{GL}318$	GL	0.234	0.271	1.0	157	2	134	255
$Q_{GL}322$	GL	0.241	0.283	1.5	152	5	137	245
$Q_{GL}326$	GL	0.246	0.268	1.8	152	6	135	245
$Q_{GL}330$	GL	0.238	0.266	1.3	154	4	132	249
$Q_{GL}334$	GL	0.238	0.271	1.4	153	4	131	247
$Q_{GL}338$	LC	0.325	0.154	3.2	125	17	155	204
$Q_{LC}318$	Int	0.279	0.225	2.7	139	12	151	227
$Q_{LC}338$	LC	0.309	0.170	3.1	128	15	154	207

[a] The successive entries include the simulation label (Table 2), the phase after 20 ns (GL, gel; LC, liquid-crystal; Int, intermediate), the area per lipid a_{xy}, the chain-averaged order parameter S_{chn}^{end}, the average number of *gauche* conformations per chain n_G, the numbers of intralayer (N_{LL}^{intra}) and interlayer (N_{LL}^{inter}) lipid−lipid H bonds, and the numbers of lipid−water N_{LW} and water−water N_{WW} H bonds.

to systems at full hydration will be considered. These simulations were initiated from structures characteristic of the GL and LC phases, respectively, and carried out at temperatures where the considered phase is thermodynamically stable (experimentally, but also within the present force field, as will be discussed in sections III.2 and III.3); i.e., these represent equilibrium simulations for the two phases considered. The average values of key properties calculated over the last 10 ns of the trajectories are shown in Tables 3 (structural properties) and 4 (dynamic properties).

The average area per lipid a_{xy} in the GL phase ($F_{GL}318$), 0.248 nm^2, is slightly higher than the experimental estimate of 0.22 nm^2 reported by Pezron et al.[61] On the other hand, the corresponding average in the LC phase ($F_{LC}338$), 0.296 nm^2, is slightly lower than the corresponding experimental estimate[61] of 0.31 nm^2. However, the small differences observed between calculated and experimental values are well within the error associated with the experimental data. Although no error bar was provided for these specific measurements,[61] similar determinations considering the area per lipid of the LC phase of DPPC have led to a range of estimates as wide as[11] 0.48−0.73 nm^2 (the most commonly accepted value being[11] 0.64 nm^2). The present simulations are thus essentially in agreement with experimental results. As expected, the chain-averaged order parameters (S_{chn}^{end}) also indicate a higher extent of ordering of the aliphatic tails in the GL phase (0.276) compared to the LC phase (0.194). The average number n_G of *gauche* conformations per chain is also higher for the LC phase (3.1) compared to the GL phase (1.6). For the LC phase, the corresponding proportion of *trans* conformers (about 75%) also agrees well with available simulation and experimental data.[48]

Due to the thickness of the hydration layer in the systems at full hydration, no interlayer lipid−lipid H bonds were observed during these simulations ($N_{LL}^{inter} = 0$). Considering the available X-ray structures of monoglycerides in the CR phase,[6−8] both of the free glycerol hydroxyl groups are involved in two lipid−lipid H bonds, one interlayer and one intralayer (no cocrystallization water molecules were observed in these crystals). Assuming that the interlayer H bonds observed in the CR phase are replaced by lipid−water H bonds in the GL phase on a one-to-one basis (as suggested by Pezron et al.[61]), the calculated numbers $N_{LL}^{intra} = 143$ and $N_{LW} = 156$ for the GL phase (i.e., almost exactly two H bonds of either type per lipid molecule) are in excellent agreement with the crystallographic observations. The number of intralayer lipid−lipid H bonds N_{LL}^{intra} is about 20% lower for the LC phase compared to the GL phase. Such a decrease is expected to result from both the temperature increase (enhanced thermal fluctuations) and the higher inherent extent of disorder in the LC phase (suboptimal headgroup orientations for H-bonding). However, concomitantly, the number of lipid−water H bonds N_{LW} is about 20% higher in the LC phase. Such a (nearly quantitative) compensation effect between changes in the number of lipid−lipid and lipid-environment H bonds upon altering the phase or environment of a bilayer (i.e., the conservation of the headgroup H-bond saturation) has been observed previously in different contexts.[87−90]

As expected, the LC phase also evidences a more pronounced fluidity compared to the GL phase. The calculated lipid lateral diffusion coefficient D_{xy} is about twice as high for the LC phase (9.4×10^{-11} m^2•s^{-1}) compared to the GL phase (4.6×10^{-11} m^2•s^{-1}). These numbers should probably be viewed as upper bounds, due to finite-size effects in the microscopic simulated systems.[55] To our knowledge, the corresponding experimental values are not known for GMP. A comparison with the experimental[91] and simulation[55] values of 1.25 and 0.95×10^{-11} m^2•s^{-1}, respectively, for DPPC indicates that the lateral diffusion of GMP molecules (single acyl chain, low polarity headgroup) is much faster than that of DPPC (two acyl chains, zwitterionic headgroup). The rotational and wobbling motions of the lipids also take place on different time scales in the two phases. In the GL phase, the rotational motion appears to involve two distinct regimes (i.e., the corresponding autocorrelation function follows a biexponential form). The first regime involves a fast decay ($\tau_1^R = 0.27$ ns), leading to a residual correlation $c_1^R = 0.12$. After a second slower decay ($\tau_2^R = 2.6$ ns), the correlation essentially reaches zero ($c_2^R = 0.03$). In contrast, for the LC phase, a single fast decay is observed ($\tau_1^R = 0.19$ ns), leading to an essentially vanishing residual correlation ($c_1^R = 0.05$). The fast motion (time scale ~0.2 ns) can be attributed to the rotation of a single lipid molecule around its axis. The slow motion (time scale ~ 2.5 ns) observed in the GL phase can be attributed to

Table 4. Dynamic Properties Calculated over the Last 10 ns (12 ns for D_{xy}) of the Simulations[a]

		rotational motion					wobbling motion			
simulation code	phase (after 20 ns)	D_{xy} [10^{-11} m^2 s^{-1}]	τ_1^R [10^2 ps]	c_1^R	τ_2^R [10^3 ps]	c_2^R	τ_1^W [10^3 ps]	c_1^W	τ_2^W [10^4 ps]	c_2^W
$F_{GL}318$	GL	4.6 ± 2.0	2.7	0.12	2.6	0.03	19.0	0.96	7.7	0.93
$F_{GL}322$	GL	5.9 ± 3.4	2.5	0.10	4.0	0.04	15.6	0.95	5.7	0.91
$F_{GL}326$	LC	8.8 ± 2.0	2.1	0.07	9.7	0.04	3.1	0.83	2.6	0.74
$F_{GL}330$	LC	10.5 ± 1.8	1.9	0.06	12.6	0.03	2.9	0.82	2.7	0.73
$F_{GL}334$	LC	10.7 ± 1.3	1.9	0.05	4.1	0.04	2.7	0.80	3.2	0.73
$F_{GL}338$	LC	13.4 ± 1.6	1.9	0.05	8.5	0.04	2.6	0.80	3.5	0.73
$F_{LC}318$	GL	2.7 ± 1.2	2.7	0.12	2.7	0.03	25.4	0.97	18.5	0.95
$F_{LC}338$	LC	9.4 ± 1.2	1.8	0.05	13.0	0.03	2.7	0.80	4.4	0.74
$H_{GL}318$	GL	3.0 ± 1.5	2.6	0.11	3.2	0.04	28.4	0.97	15.2	0.96
$H_{GL}322$	GL	2.1 ± 0.4	2.3	0.09	2.9	0.03	21.5	0.96	9.5	0.94
$H_{GL}326$	GL	4.3 ± 2.5	2.2	0.08	3.1	0.02	16.6	0.96	8.7	0.93
$H_{GL}330$	GL	4.1 ± 2.1	2.1	0.07	5.4	0.04	15.0	0.95	14.2	0.93
$H_{GL}334$	LC	6.9 ± 1.5	2.0	0.06	5.8	0.03	2.8	0.82	2.1	0.72
$H_{GL}338$	LC	7.8 ± 1.3	1.9	0.06	187.1	0.04	2.3	0.78	2.5	0.69
$H_{LC}318$	Int	4.8 ± 0.7	2.6	0.11	3.2	0.03	3.9	0.86	2.2	0.76
$H_{LC}338$	LC	8.4 ± 1.4	1.8	0.05	36.7	0.04	2.2	0.78	2.1	0.68
$Q_{GL}318$	GL	1.6 ± 0.1	2.8	0.13	2.1	0.03	73.2	0.99	394.4	0.98
$Q_{GL}322$	GL	1.8 ± 0.3	2.8	0.13	2.4	0.04	21.6	0.96	8.2	0.93
$Q_{GL}326$	GL	1.5 ± 0.3	2.5	0.11	1.9	0.03	16.8	0.96	11.8	0.93
$Q_{GL}330$	GL	1.4 ± 0.4	2.4	0.10	1.6	0.01	36.0	0.97	18.4	0.96
$Q_{GL}334$	GL	1.5 ± 0.3	2.0	0.06	3.2	0.02	60.9	0.98	831.9	0.98
$Q_{GL}338$	LC	5.6 ± 0.3	2.2	0.08	9.5	0.03	2.6	0.80	1.5	0.67
$Q_{LC}318$	Int	2.9 ± 0.1	3.3	0.17	1.9	0.04	4.3	0.87	2.4	0.78
$Q_{LC}338$	LC	5.6 ± 0.9	2.3	0.08	11.5	0.05	2.4	0.79	1.8	0.68

[a] The successive entries include the simulation label (Table 2), the phase after 20 ns (GL, gel; LC, liquid-crystal; Int, intermediate), the lipid lateral diffusion coefficient D_{xy}, the first (τ_1^R) and second (τ_2^R) relaxation times corresponding to the two observed decays in the rotational motion with corresponding residual correlations (c_1^R and c_2^R), and the first (τ_1^W) and second (τ_2^W) relaxation times corresponding to the two observed decays in the wobbling motion with corresponding residual correlations (c_1^W and c_2^W).

correlated motions within a bilayer leaflet, such as the reorientation (precession) of the lipid tilting angle within the leaflet. The wobbling motion exhibits two decay regimes with high residual correlations, as expected for a vector that does not sample the accessible space isotropically (i.e., the aliphatic tails always point preferentially from the headgroup plane toward the membrane midplane). For the GL phase, the two decays are slow ($\tau_1^W = 19$ ns, $\tau_2^W = 77$ ns) and result in a very high residual correlation ($c_2^W = 0.96$). For the LC phase, the relaxation times for both decays are shorter ($\tau_1^W = 2.7$ ns, $\tau_2^W = 44$ ns), and the final residual correlation is comparatively smaller ($c_2^W = 0.74$), again indicative of a more limited tail ordering in this phase.

III.2. GL ↔ LC Transition: Reversibility. The reversibility of the GL ↔ LC phase transition (at the three levels of hydration) will be discussed considering the simulations initiated from structures appropriate for the GL or LC phases and performed at two different temperatures, 318 and 338 K (i.e., corresponding, respectively, to 10 K below and 10 K above the experimental $T_m = 328$ K at full hydration;[69] Figure 2). The presence of a transition can be assessed by monitoring the time series of the area per lipid a_{xy} and of the chain-averaged order parameter S_{chn}. These time series are displayed in Figure 3 for the simulations at full hydration, half hydration, and quarter hydration. The average values of key properties calculated over the last 10 ns of the trajectories are also reported in Tables 3 (structural properties) and 4 (dynamic properties).

The time evolutions of a_{xy} and of S_{chn} are clearly anticorrelated, both in terms of net changes (for systems undergoing a GL ↔ LC phase transition) and in terms of fluctuations (within time periods corresponding to a single phase). In other words, an increase (decrease) in the area per lipid always occurs concomitantly with a decrease (increase) in the ordering of the lipid tails. All simulations initiated from structures appropriate for the GL or LC phase and carried out within the temperature range in which the corresponding phase is expected to be stable (318 K for GL and 338 K for LC) do not evidence transitions, which justifies the equilibrium analysis of section III.1. In contrast, complete or incomplete transitions are observed in the simulations initiated from structures appropriate for the GL or LC phase and carried out at a temperature where the alternative phase is expected to be more stable (GL → LC at 338 K and LC → GL at 318 K; for simulations $H_{LC}318$ and $Q_{LC}318$, the transitions are incomplete on the 40 ns time scale, see below).

For the systems at full hydration (Figure 3a), the GL phase is stable at 318 K ($F_{GL}318$) with very limited fluctuations of a_{xy} and S_{chn}. The corresponding average values (last 10 ns) are 0.248 nm^2 and 0.276, respectively (Table 3). The LC phase is stable at 338 K ($F_{LC}338$), but a_{xy} and S_{chn} undergo larger fluctuations due to the enhanced thermal fluctuations. The corresponding average values (last 10 ns) are 0.296 nm^2 and 0.194. The systems $F_{GL}338$ and $F_{LC}318$ are not at equilibrium in their starting phase and undergo a transition, as expected. The simulation initiated with a structure appropriate for the GL phase and carried out above the phase transition temperature ($F_{GL}338$) evidences changes in a_{xy} from about 0.25 to about 0.30 nm^2 and in S_{chn} from about 0.27 to about 0.20 within the first 10 ns. Conversely, the simulation initiated with a structure appropriate for the LC phase and carried out below the phase transition temperature ($F_{LC}318$)

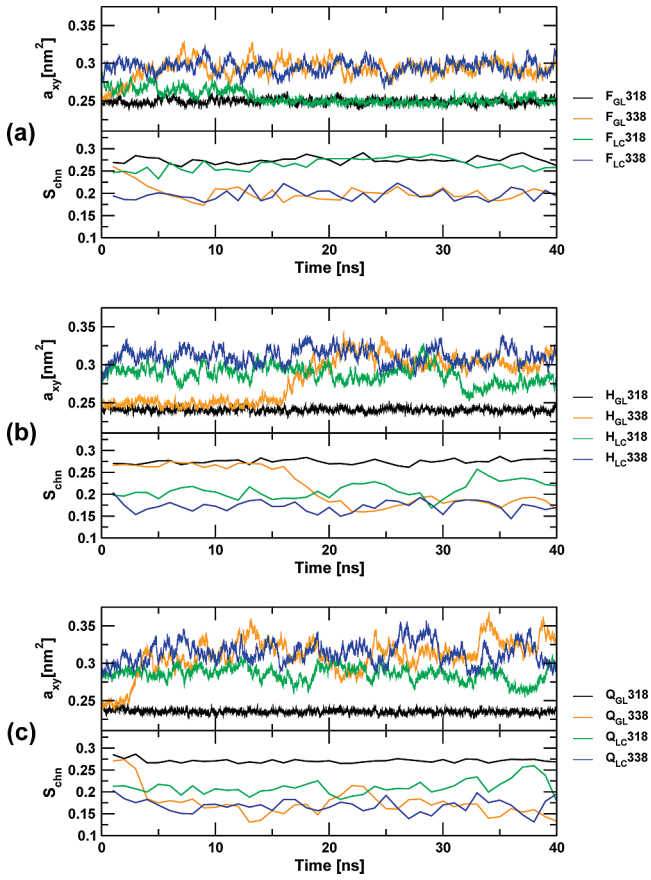

Figure 3. Time series of the area per lipid a_{xy} and of the chain-averaged order parameters S_{chn} for the simulations initiated from a structure appropriate for the GL or the LC phase and carried out at temperatures of 318 or 338 K. The three panels correspond to different hydration levels: (a) full hydration, (b) half hydration, and (c) quarter hydration. See Table 2 for the simulation labels.

evidences changes in a_{xy} from about 0.30 to about 0.25 nm^2 and in S_{chn} from about 0.20 to about 0.27 within the first 15 ns.

For the systems at half hydration (Figure 3b), the GL phase is stable at 318 K ($H_{GL}318$), and the LC phase is stable at 338 K ($H_{LC}338$). These two simulations are very similar to the corresponding simulations at full hydration ($F_{GL}318$ and $F_{LC}338$) in terms of all simulated properties (Figure 3, Tables 3 and 4). The simulation initiated from a structure appropriate for the GL phase and carried out above the phase transition temperature ($H_{GL}338$) evidences changes in a_{xy} from about 0.25 to about 0.30 nm^2 and in S_{chn} from about 0.27 to about 0.20 in the interval 15−20 ns. In contrast to the situation at full hydration, however, the simulation initiated from a structure appropriate for the LC phase and carried out below the phase transition temperature ($H_{LC}318$) evidences a progressive change in a_{xy} and S_{chn} in the direction of the GL phase values but does not reach converged values within the simulation time scale of 40 ns. As a result, at the end of the simulation, an intermediate state (the properties of which lie between those of the GL and LC phases) is reached (Tables 3 and 4). To verify that the incompleteness of the transition is due to kinetic (and not thermodynamic) factors, simulation $H_{LC}318$ was further extended to 200 ns (data not shown). The transition was found to occur after about 94 ns.

For the systems at quarter hydration (Figure 3c), the GL phase is stable at 318 K ($Q_{GL}318$), and the LC phase is stable at 338 K ($Q_{LC}338$). The transition from the GL to the LC phase ($Q_{GL}338$) also occurs, this time at the very beginning of the simulation. However, as for the corresponding simulation at half hydration, the simulation from the LC to the GL phase ($Q_{LC}318$) does not entirely converge within 40 ns and reaches an intermediate state. Here also, simulation $Q_{LC}318$ was extended to 200 ns (data not shown), and the LC → GL transition was found to occur after about 144 ns.

In summary, simulations on the 40 ns time scale are able to capture the reversible interconversion between the two phases and the correct transition temperature under conditions of full hydration. At lower hydration, the GL → LC transition can be appropriately simulated on this time scale, but the LC → GL transition appears to require significantly longer simulations (by about a factor five). The dependence of the transition temperature on the hydration level will be discussed in section III.3.

The present simulations suggest that the GL → LC transition tends to occur on a shorter time scale compared to the LC → GL transition. This difference is not visible at full hydration but is clearly observed for the systems at lower hydration. Two effects may be invoked to explain this difference. First, the LC phase is stable at higher temperatures compared to the GL phase. Thus, in order to promote a GL → LC transition, a system with a GL structure is heated up to a temperature above the phase transition temperature. In contrast, to promote a LC → GL transition, a system with a LC structure is cooled down to a temperature below the phase transition temperature. The second process is likely to be slower, as a direct consequence of the lower (average) atomic velocities in the simulation. Second, the GL phase is a more ordered phase compared to the LC phase. As a result, the LC → GL transition is expected to involve a high entropic barrier; i.e., the lipid molecules must sample a large extent of conformational space before reaching the regular arrangement characteristic of the GL phase. This process is also slowed down by the reduction of the area per lipid (packing constraints) and by the concomitant decrease in the lipid translational and rotational diffusion. (Table 4). In contrast, the GL → LC transition is expected to involve a comparatively much lower entropic barrier, due to the entropy increase of the overall process. The observation that the time scale associated with the LC → GL transition tends to increase when the hydration level is decreased is certainly related to the associated increase in the viscosity of the system. For example, the lipid lateral diffusion coefficient systematically decreases upon reducing the water content of the system, for both the GL and LC phases (Table 4).

Note, finally, that even for the simulations where a complete GL → LC ($F_{GL}338$, $H_{GL}338$, $Q_{GL}338$) or LC → GL ($F_{LC}318$) transition is observed, some properties might not be entirely converged after the transition given the 40 ns time scale of the simulations, as evidenced by comparison with the corresponding equilibrium simulations ($F_{LC}338$, $H_{LC}338$, $Q_{LC}338$, and $F_{GL}318$), see Tables 3 and 4.

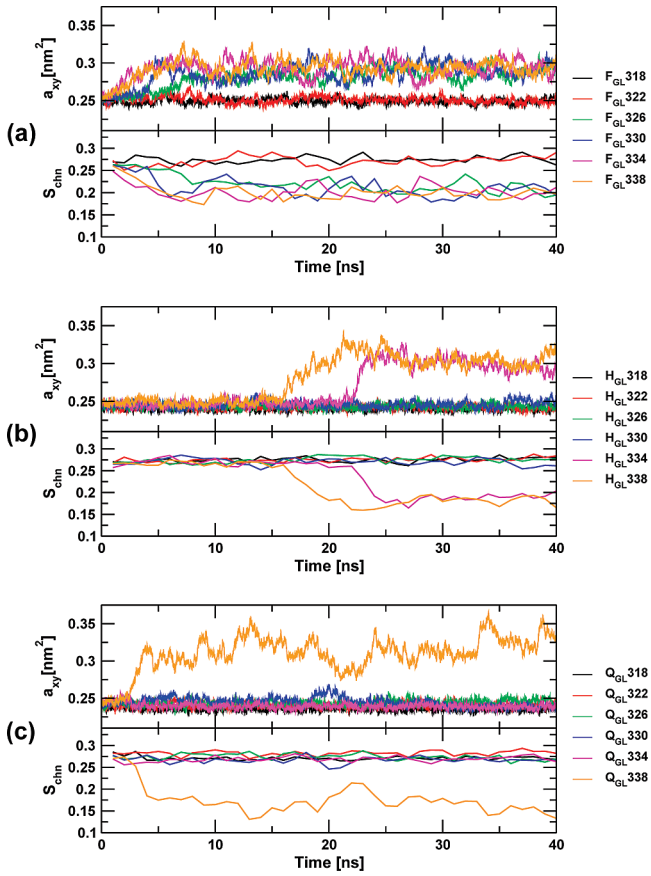

Figure 4. Time series of the area per lipid a_{xy} and of the chain-averaged order parameters S_{chn} for the simulations initiated from a structure appropriate for the GL phase and carried out at temperatures of 318, 322, 326, 330, 334, or 338 K. The three panels correspond to different hydration levels: (a) full hydration, (b) half hydration, and (c) quarter hydration. See Table 2 for the simulation labels.

III.3. GL → LC Transition: Temperature vs Hydration. Considering the above results, the determination of the lowest temperature for which a GL → LC transition is observed on the 40 ns time scale appears to provide a reliable method for the evaluation of the phase transition temperature T_m. Of course, a bracketing using the highest temperature for which a LC → GL transition is observed would be desirable but remains at present computationally too demanding (requiring simulations longer by at least a factor five).

The dependence of the transition temperature T_m on the level of hydration will thus be investigated considering the 18 simulations initiated from a structure appropriate for the GL phase at the three different hydration levels and carried out at distinct temperatures with a 4 K interval in the range 318−338 K. The corresponding time series of the area per lipid a_{xy} and of the chain-averaged order parameter S_{chn} are displayed in Figure 4.

At full hydration (Figure 4a), the simulations $F_{GL}318$ and $F_{GL}322$ remain stable in the GL phase during the entire trajectory, while the simulations $F_{GL}326$−$F_{GL}338$ evidence a transition to the LC phase within the first 10 ns. After 10 ns, the two sets of curves are clearly separated, suggesting that they both correspond to systems having reached their equilibrium phase at the given temperature. At half hydration (Figure 4b), the simulations $H_{GL}318$−$H_{GL}330$ remain stable in the GL phase during the entire trajectory, while the simulations $H_{GL}334$ and $H_{GL}338$ evidence a transition to the LC phase after about 23 and 20 ns, respectively. Here also, the two sets of curves are well separated after the first 25 ns. Finally, at quarter hydration (Figure 4c), the simulations $Q_{GL}318$−$Q_{GL}334$ remain stable in the GL phase and the only simulation evidencing a transition to the LC phase after about 4 ns is $Q_{GL}338$. Here again, the latter curve remains well separated from the five others after the first 5 ns.

The order parameters $S_{CH}(C_n)$ of the 14 methylene groups (C_n, $n = 2-15$) within the aliphatic tails calculated over the last 10 ns of the trajectories are shown in Figure 5. The average values of key properties calculated over the same interval are reported in Tables 3 (structural properties) and 4 (dynamic properties).

Overall, on the basis of these final properties, the simulations can unambiguously be classified into two distinct groups, depending on whether the GL → LC transition has occurred or not during the simulation. Residual differences between the different simulations within the two groups are due to the slightly different simulation temperatures, to the limited averaging time, and in the cases where a GL → LC transition has occurred, to insufficient equilibration after the transition (as mentioned in section III.2). These residual differences are least pronounced for simulations $F_{GL}318$ and $F_{GL}322$ (full hydration, no transition), except for a slightly higher diffusivity (lateral, rotational, wobbling) of the lipids in the latter case. They are slightly more important for simulations $F_{GL}326$−$F_{GL}338$ (full hydration, GL → LC transition), where the order parameters systematically decrease and the diffusivity of the lipids slightly increases upon increasing the temperature. Simulations $H_{GL}318$−$H_{GL}330$ (half hydration, no transition) show limited differences, except for noticeably lower order parameters at 330 K and a slight systematic increase in the diffusivity of the lipids upon increasing the temperature. Simulations $H_{GL}334$ and $H_{GL}338$ (half hydration, GL → LC transition) show similar trends to those of the corresponding simulations at full hydration ($F_{GL}326$−$F_{GL}338$). Simulations $Q_{GL}318$−$Q_{GL}334$ (quarter hydration, no transition) show similar trends to those of the corresponding simulations at half hydration ($H_{GL}318$−$H_{GL}330$). Finally, simulation $Q_{GL}338$ is the only one undergoing a phase transition at this hydration level.

Comparing the GL and the LC phases (see also section III.1), the former is characterized by significantly higher order parameters and a significantly lower diffusivity (lateral, rotational, wobbling) of the lipids. In general, a decrease in the hydration level tends to promote (*i*) a slight decrease in the order parameters for the GL phase, (*ii*) a somewhat more pronounced decrease in the order parameters for the LC phase, (*iii*) a slight decrease in the number of *gauche* conformations per chain for the GL phase, (*iv*) a significant decrease in the diffusivity (lateral, rotational, wobbling) of the lipids. By decreasing the hydration level, the thickness of the water layer between successive (periodic) bilayers decreases, and the H-bonded interaction of one leaflet with a periodic image of the other leaflet becomes possible. As a

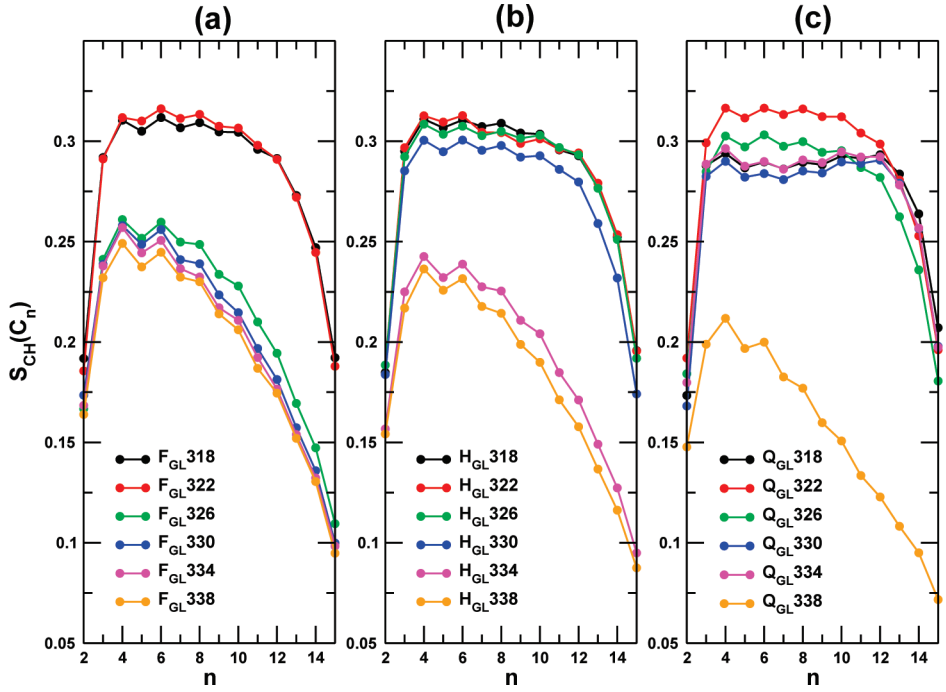

Figure 5. Order parameters $S_{CH}(C_n)$ of the 14 methylene groups (C_n, $n = 2-15$) calculated considering the last 10 ns of the simulations initiated from a structure appropriate for the GL phase and carried out at temperatures of 318, 322, 326, 330, 334, or 338 K. The three panels correspond to different hydration levels: (a) full hydration, (b) half hydration, and (c) quarter hydration. See Table 2 for the simulation labels.

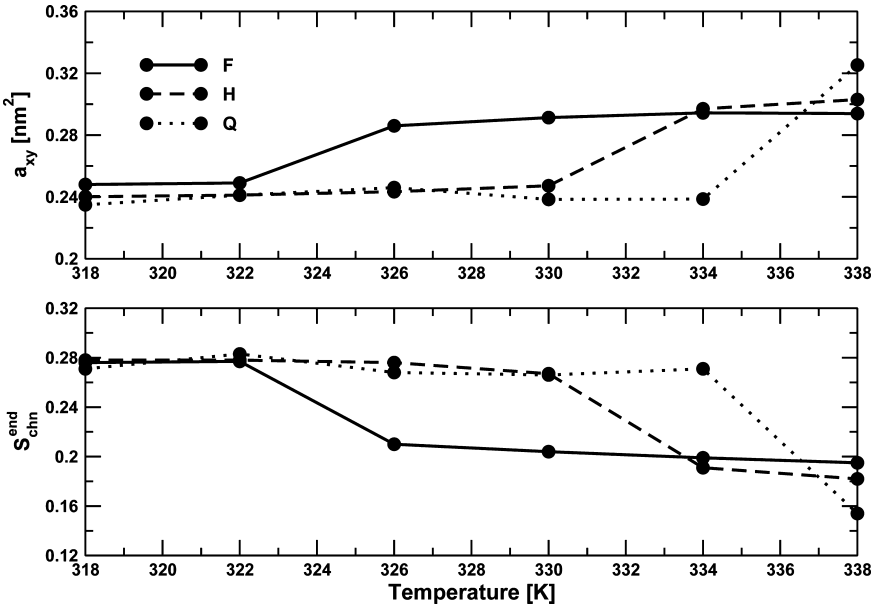

Figure 6. Average area per lipid a_{xy} (top panel) and chain-averaged order parameter S^{end}_{chn} (bottom panel) calculated considering the last 10 ns of the simulations initiated from a structure appropriate for the GL phase and carried out at different temperatures. The different linestyles correspond to the three considered hydration levels: full (F), half (H), and quarter (Q) hydration.

consequence, interlayer H bonds (N^{inter}_{LL}) are observed at half and, more markedly, quarter hydration. The presence of these H bonds represents an artifact of the simulation setup when taking the single-bilayer experiment as a reference. However, they are expected to occur in multilamellar systems. Finally, the H-bond compensation effect discussed in section III.1 (conservation of $N^{intra}_{LL} + N^{inter}_{LL} + N_{LW}$) is observed for all of the simulations evidencing a GL → LC transition.

On the basis of the above observations, the final values of the area per lipid a_{xy} and of the chain-averaged order parameters S^{end}_{chn} in the simulations may serve as an indicator for the most stable phase at a given temperature T. The corresponding results are displayed graphically in Figure 6. They suggest ranges for the transition temperature T_m of 322−326, 330−334, and 334−338 K in the systems at full, half, and quarter hydration, respectively. Considering the corresponding hydration levels (30.5, 18.2, and 9.1% w/w, respectively) these estimated transition temperatures (midpoints at 51, 59, and 63 °C, respectively) agree qualitatively very well with the experimental phase diagram[69] of GMP

(Figure 2; experimental T_m of about 50, 53, and 58 °C), and even essentially quantitatively given an estimated error of 2 °C on the simulation values and of 4 °C on the experimental ones (considering that the independent studies of refs 69 and 92 report T_m at full hydration of 50 and 54, respectively).

IV. Conclusion

The goal of the present study was to investigate whether atomistic MD simulations on the 10−100 ns time scale could be used to monitor GL ↔ LC transitions in lipid bilayers, and to evaluate the corresponding transition temperatures T_m (as well as environmental influences on T_m) in a reliable fashion. This time scale is possibly still too short in the context of lipids such as DPPC (two acyl tails, zwitterionic headgroup), in view of the slow translational and rotational relaxation of the lipid molecules in this case. For this reason, the simpler monoglyceride lipid GMP (one acyl tail, lower polarity headgroup) was considered instead in the present work. To our knowledge, this study represents the first investigation of GMP bilayers by simulation.

The main results of this work can be summarized as follows. First, simulations of 40 ns are able to account for the GL → LC transition and for the presence of a threshold temperature associated with this transition; i.e., they can provide a lower bound for T_m. Thus, by performing a set of simulations initiated from a structure appropriate for the GL phase and carried out at slightly different temperatures, it is possible to evaluate T_m accurately (here, within an interval of 4 °C). Simulations on longer time scales (about 200 ns) appear to be required for the inverse LC → GL transition, especially at water contents lower than full hydration. Although such simulations were not performed here in a systematic fashion, they could in principle provide another threshold temperature, i.e., an upper bound for T_m. The observation that the LC → GL transition is slower than the GL → LC transition is reasonable, considering that the former transition is a disorder → order transition (high entropy barrier). Second, an investigation of the influence of the hydration level (full, half, or quarter hydration) on the calculated T_m value could evidence the experimentally expected increase in this transition temperature upon decreasing the bilayer hydration. Another interesting observation is that in general, a decrease in the hydration level tends to promote a decrease in the order parameters as well as in the diffusivity (lateral, rotational, wobbling) of the lipids for both the GL and LC phases (the order parameters are themselves higher for the GL phase while the diffusivity is higher for the LC phase). Third, the T_m values calculated at the three hydration levels considered are in remarkable (qualitative and even essentially quantitative) agreement with the experimental phase diagram of GMP.[69] Qualitative agreement indicates that the model underlying the simulations (force field) is able to capture the essential physics of the system. Quantitative agreement, although pleasant, is probably largely fortuitous considering the approximations involved in this model and the empirical nature of its parameters.

To our knowledge, this study represents the first accurate determination of the T_m of a lipid *via* atomistic simulations of the (reversible) GL ↔ LC phase transition, as well as the first direct simulation evidence for the increase in the transition temperature upon dehydration. The direct determination of T_m by simulation is of high relevance in the context of force field development. The reason is that T_m typically represents one of the most accurately known experimental properties of the lipid−water system for a given lipid type. It would usefully complement the few other quantities available for the parametrization of a force field (transverse electron density profile and area per lipid, the latter being sometimes affected by a considerable experimental uncertainty). The investigation of the influence of hydration on the T_m value is also of great interest in the context of dehydration-induced damages in living cells and bioprotection by cosolutes.[19−26]

Important extensions of the present approach include (*i*) investigation of the feasibility of monitoring GL ↔ LC transitions in more complex (and biologically relevant) lipids such as DPPC (involving simulations on significantly longer time scales) and (*ii*) investigation of the influence of other environmental factors (besides hydration) on T_m (e.g., concentration of biologically relevant cosolutes[90] such as electrolytes, alcohols, anesthetics, or sugars). A particularly interesting example of a cosolute is the bioprotective sugar trehalose, which is known to depress the T_m of lipid bilayers at low hydration, thereby counteracting the potentially damaging T_m increase observed above.[87] Further extensions of this work along the two above lines are in progress.

Acknowledgment. Financial support from the Swiss National Science Fundation (Grant 21-121895) is gratefully acknowledged.

References

(1) Seddon, J. M.; Cevc, G. Lipid polymorphism: Structure and stability of lyotropic mesophases of phospholipids. In *Phospholipids Handbook*; Cevc, G., Ed.; Marcel Dekker, Inc.: New York, 1993; pp 403−454.

(2) Foubert, I.; Dewettinck, K.; Van de Walle, D.; Dijkstra, A. J.; Quinn, P. J. Physical Properties: Structural and Physical Characteristics. In *The Lipid Handbook*, 3rd ed.; Gunstone, F. D., Harwood, J. L., Dijkstra, A. J., Eds.;CRC Press, Div. of Taylor, Francis Group: Boca Raton, FL, 2007; pp 471−534.

(3) Jensen, L. H.; Mabis, A. J. *Acta Crystallogr.* **1966**, *21*, 770–781.

(4) Pascher, I.; Lundmark, M.; Nyholm, P.-G.; Sundell, S. *Biochim. Biophys. Acta* **1992**, *1113*, 339–373.

(5) Pascher, I. *Curr. Opin. Struct. Biol.* **1996**, *6*, 439–448.

(6) Larsson, K. *Acta Crystallogr.* **1966**, *21*, 267–272.

(7) Goto, M.; Kozo, K. *Bull. Chem. Soc. Jpn.* **1988**, *61*, 1434–1436.

(8) Goto, M.; Takiguchi, T. *Bull. Chem. Soc. Jpn.* **1985**, *58*, 1319–1320.

(9) Larsson, K. *Ark. Kemi* **1964**, *23*, 35–56.

(10) Dorset, D. L.; Pangborn, W. A.; Hancock, A. J.; van Soest, T. C. *Z. Naturforsch.* **1978**, *33c*, 50–55.

(11) Nagle, J. F.; Tristram-Nagle, S. *Biochim. Biophys. Acta* **2000**, *1469*, 159–195.

(12) Risselada, H. J.; Marrink, S. J. *Proc. Natl. Acad. Sci. U.S.A.* **2008**, *105*, 17367–17372.

(13) Marrink, S. J.; Risselada, J.; Mark, A. E. *Chem. Phys. Lipids* **2005**, *135*, 223–244.

(14) Brown, D. A.; London, E. *Annu. Rev. Cell Dev. Biol.* **1998**, *14*, 111–136.

(15) Simons, K. *Nature* **1997**, *387*, 569–572.

(16) Simons, K.; Toomre, D. *Nat. Rev. Mol. Cell. Biol.* **2000**, *1*, 31–40.

(17) Herreros, J.; Ng, T.; Schiavo, G. *Mol. Biol. Cell* **2001**, *12*, 2947–2960.

(18) Keilin, D. *Proc. R. Soc. London, Sect. B* **1959**, *150*, 149–191.

(19) Clegg, J. S. *Comp. Biochem. Physiol.* **2001**, *128B*, 613–624.

(20) Feovilova, E. P. *Appl. Biochem. Microbiol.* **2003**, *39*, 1–18.

(21) Zhmakin, A. I. *Physics—Uspekhi* **2008**, *51*, 231–252.

(22) Crowe, J. H.; Hoekstra, F. A.; Crowe, L. M. *Annu. Rev. Physiol.* **1992**, *54*, 579–599.

(23) Guppy, M.; Withers, P. *Biol. Rev.* **1999**, *74*, 1–40.

(24) Crowe, J. H.; Crowe, L. M.; Wolkers, W. F.; Oliver, A. E.; Ma, X.; Auh, J.-H.; Tang, M.; Zhu, S.; Norris, J.; Tablin, F. *Integr. Comp. Biol.* **2005**, *45*, 810–820.

(25) Hengherr, S.; Heyer, A. G.; Koehler, H. *FEBS J.* **2008**, *275*, 281–288.

(26) Crowe, L. M. *Comp. Biochem. Physiol.* **2002**, *131A*, 505–513.

(27) Treanor, R. L.; Weiss, R. G. *J. Am. Chem. Soc.* **1988**, *110*, 2170–2177.

(28) Ariga, K; Nakanishi, T.; Kawanami, S.-I.; Kosaka, T.; Kikuchi, *J. Nanosci. Nanotechnol.* **2006**, *6*, 1718–1730.

(29) Horváth, R.; Fricsovszky, G.; Papp, E. *Biosens. Bioelectron.* **2003**, *18*, 415–428.

(30) Liu, J.; Conboy, J. C. *J. Am. Chem. Soc.* **2004**, *126*, 8894–8895.

(31) Alaouie, A. M.; Smirnov, A. I. *J. Magn. Reson.* **2006**, *182*, 229–238.

(32) Jähnig, F. *Biophys. J.* **1996**, *71*, 1348–1349.

(33) Roux, B. *Biophys. J.* **1996**, *71*, 1346–1347.

(34) Tieleman, D. P.; Berendsen, H. J. C. *J. Chem. Phys.* **1996**, *105*, 4871–4880.

(35) Tieleman, D. P.; Marrink, S. J.; Berendsen, H. J. C. *Biochim. Biophys. Acta* **1997**, *1331*, 235–270.

(36) Cantor, R. S. *Biophys. J.* **1999**, *76*, 2625–2639.

(37) Feller, S. E.; Pastor, R. W. *J. Chem. Phys.* **1999**, *111*, 1281–1287.

(38) Feller, S. E. *Curr. Opin. Colloid Interface Sci.* **2000**, *5*, 217–223.

(39) Chandrasekhar, I.; Bakowies, D.; Glättli, A.; Hünenberger, P. H.; Pereira, C.; van Gunsteren, W. F. *Mol. Simul.* **2005**, *31*, 543–548.

(40) Heller, H.; Schaefer, M.; Schulten, K. *J. Phys. Chem.* **1993**, *97*, 8343–8360.

(41) Essmann, U.; Perera, L.; Berkowitz, M. L. *Langmuir* **1995**, *11*, 4519–4531.

(42) Venable, R. M.; Brooks, B. R.; Pastor, R. W. *J. Chem. Phys.* **2000**, *112*, 4822–4832.

(43) Tobias, D. J.; Tu, K.; Klein, M. L. *Curr. Opin. Colloid Interface Sci.* **1997**, *2*, 15–26.

(44) de Vries, A. H.; Yefimov, S.; Mark, A. E.; Marrink, S. J. *Proc. Natl. Acad. Sci.* **2005**, *102*, 5392–5396.

(45) Marrink, S. J.; Tieleman, D. P. *J. Am. Chem. Soc.* **2001**, *123*, 12383–12391.

(46) Fuhrmans, M.; Knecht, V.; Marrink, S. J. *J. Am. Chem. Soc.* **2009**, *131*, 9166–9167.

(47) Leermakers, F. A. M.; Scheutjens, J. M. H. M. *J. Chem. Phys.* **1988**, *89*, 6912–6924.

(48) Takaoka, Y.; Pasenkievicz-Gierula, M.; Miyagawa, H.; Kitamura, K.; Tamura, Y.; Kusumi, A. *Biophys. J.* **2000**, *79*, 3118–3138.

(49) Debnath, A.; Ayappa, K. G.; Kumaran, V.; Maiti, P. K. *J. Phys. Chem. B* **2009**, *113*, 10660–10668.

(50) Reif, M. M.; Krutler, V.; Kastenholz, M. A.; Daura, X.; Hünenberger, P. H. *J. Phys. Chem. B* **2009**, *113*, 3112–3128.

(51) Anézo, C.; de Vries, A. H.; Höltje, H.-D.; Tieleman, D. P.; Marrink, S.-J. *J. Phys. Chem. B* **2003**, *107*, 9424–9433.

(52) Baştuğ, T. P.; Kuyucak, S. M. *Chem. Phys. Lett.* **2006**, *425*, 320–323.

(53) Cordomi, A.; Edholm, O.; Perez, J. *J. Comput. Chem.* **2007**, *28*, 1017–1030.

(54) Herce, D. H.; Garcia, A. E. *J. Chem. Phys.* **2006**, *125*, 224711/1−224711/13.

(55) Klauda, J. B.; Brooks, B. R.; Pastor, R. W. *J. Chem. Phys.* **2006**, *125*, 144710/1−144710/8.

(56) Patra, M.; Karttunen, M.; Hyvnen, M. T.; Falck, E.; Lindqvist, P.; Vattulainen, I. *Biophys. J.* **2003**, *84*, 3636–3645.

(57) Patra, M.; Karttunen, M.; Hyvönen, M. T.; Falck, E.; Vattulainen, I. *J. Phys. Chem. B* **2004**, *108*, 4485–4494.

(58) Tieleman, D. P.; Hess, B.; Sansom, M. S. P. *Biophys. J.* **2002**, *83*, 2393–2407.

(59) de Vries, A. H.; Chandrasekhar, I.; van Gunsteren, W. F.; Hünenberger, P. H. *J. Phys. Chem. B* **2005**, *109*, 11643–11652.

(60) Krog, N.; Borup, A. P. *J. Sci. Food. Agric.* **1973**, *24*, 691–701.

(61) Pezron, I.; Pezron, E.; Bergenstahl, B. A.; Claesson, P. M. *J. Phys. Chem.* **1990**, *94*, 8255–8261.

(62) Pezron, I.; Pezron, E.; Claesson, P. M.; Bergenstahl, B. A. *J. Colloid Interface Sci.* **1991**, *144*, 449–457.

(63) Morley, W. G.; Tiddy, G. J. T. *J. Chem. Soc. Faraday Trans.* **1993**, *89*, 2823–2831.

(64) Cassin, G.; de Costa, C.; van Duynhoven, J. P. M.; Agterof, W. G. M. *Langmuir* **1998**, *14*, 5757–5763.

(65) Chupin, V.; Boots, J.-W. P.; Killian, J. A.; Demel, R. A.; de Kruijff, B. *Chem. Phys. Lipids* **2001**, *109*, 15–28.

(66) Sein, A.; Verheij, J. A.; Agterof, W. G. M. *J. Colloid Interface Sci.* **2002**, *249*, 412–422.

(67) van Duynhoven, J. P. M.; Broekmann, I.; Sein, A.; van Kempen, G. M. P.; Goudappel, G.-J. W.; Veeman, W. S. *J. Colloid Interface Sci.* **2005**, *285*, 703–710.

(68) Alberola, C.; Blümich, B.; Emeis, D.; Wittern, K.-P. *Colloids Surf., A* **2006**, *290*, 247–255.

(69) Krog, N.; Larsson, K. *Chem. Phys. Lipids* **1968**, *2*, 129–143.

(70) van Gunsteren, W. F.; Billeter, S. R.; Eising, A. A.; Hünenberger, P. H.; Krüger, P.; Mark, A. E.; Scott, W. R. P.; Tironi, I. G. *Biomolecular Simulation: The GROMOS96 Manual and User Guide*; Verlag der Fachvereine: Zürich, Switzerland, 1996.

(71) Scott, W. R. P.; Hünenberger, P. H.; Tironi, I. G.; Mark, A. E.; Billeter, S. R.; Fennen, J.; Torda, A. E.; Huber, T.; Krüger, P.; van Gunsteren, W. F. *J. Phys. Chem. A* **1999**, *103*, 3596–3607.

(72) Oostenbrink, C.; Villa, A.; Mark, A. E.; van Gunsteren, W. F. *J. Comput. Chem.* **2004**, *25*, 1656–1676.

(73) Berendsen, H. J. C.; Postma, J. P. M.; van Gunsteren, W. F.; Hermans, J. Interaction models for water in relation to protein hydration. In *Intermolecular Forces*; Pullman, B., Ed.; Reidel: Dordrecht, The Netherlands, 1981; pp 331−342.

(74) Horta, B. A. C.; van Gunsteren, W. F.; Hünenberger, P. H. To be submitted to *J. Chem. Theory Comput.* **2010**.

(75) Hockney, R. W. *Methods Comput. Phys.* **1970**, *9*, 136–211.

(76) Ryckaert, J.-P.; Ciccotti, G.; Berendsen, H. J. C. *J. Comput. Phys.* **1977**, *23*, 327–341.

(77) Berendsen, H. J. C.; Postma, J. P. M.; van Gunsteren, W. F.; Di Nola, A.; Haak, J. R. *J. Chem. Phys.* **1984**, *81*, 3684–3690.

(78) Klauda, J. B.; Venable, R. M.; MacKerell, A. D., Jr.; Pastor, R. W. *Curr. Top. Membr.* **2008**, *60*, 1–48.

(79) van Gunsteren, W. F.; Berendsen, H. J. C. *Angew. Chem., Int. Ed.* **1990**, *29*, 9921023.

(80) Barker, J. A.; Watts, R. O. *Mol. Phys.* **1973**, *26*, 789–792.

(81) Tironi, I. G.; Sperb, R.; Smith, P. E.; van Gunsteren, W. F. *J. Chem. Phys.* **1995**, *102*, 5451–5459.

(82) Heinz, T. N.; van Gunsteren, W. F.; Hünenberger, P. H. *J. Chem. Phys.* **2001**, *115*, 1125–1136.

(83) Horta, B. A. C.; Perić-Hassler, L., Hünenberger, P. H. *J. Mol. Graph. Model.* **2010**, submitted.

(84) Cornell, W. D.; Cieplak, P.; Bayly, C. I.; Gould, I. R.; Merz, K. M.; Ferguson, D. M.; Spellmeyer, D. C.; Fox, T.; Caldwell, J. W.; Kollman, P. A. *J. Am. Chem. Soc.* **1995**, *117*, 5179–5197.

(85) Berendsen, H. J. C. *Simulating the Physical World*; Cambridge University Press: Cambridge, U.K., 2007.

(86) Essmann, U.; Berkowitz, M. L. *Biophys. J.* **1999**, *76*, 2081–2089.

(87) Pereira, C. S.; Lins, R. D.; Chandrasekhar, I.; Freitas, L. C. G.; Hünenberger, P. H. *Biophys. J.* **2004**, *86*, 2273–2285.

(88) Pereira, C. S.; Hünenberger, P. H. *J. Phys. Chem. B* **2006**, *110*, 15572–15581.

(89) Pereira, C. S.; Hünenberger, P. H. *Biophys. J.* **2008**, *95*, 3525–3534.

(90) Pereira, C. S.; Hünenberger, P. H. *Mol. Simul.* **2008**, *34*, 403–420.

(91) Vaz, W. L. C.; Clegg, R. M.; Hallmann, D. *Biochemistry* **1985**, *24*, 781–786.

(92) Larsson, K. *Chem. Phys. Lipids* **1972**, *10*, 177–180.

CT100200W